

# RNN-based Generative Model for Fine-Grained Sketching

Andrin Jenal, Nikolay Savinov, Torsten Sattler, and Gaurav Chaurasia

ETH Zurich

**Abstract.** Deep generative models have shown great promise when it comes to synthesising novel images. While they can generate images that look convincing on a higher-level, generating fine-grained details is still a challenge. In order to foster research on more powerful generative approaches, this paper proposes a novel task: generative modelling of 2D tree skeletons. Trees are an interesting shape class because they exhibit complexity and variations that are well-suited to measure the ability of a generative model to generate detailed structures. We propose a new dataset for this task and demonstrate that state-of-the-art generative models fail to synthesise realistic images on our benchmark, even though they perform well on current datasets like MNIST digits. Motivated by these results, we propose a novel network architecture based on combining a variational autoencoder using Recurrent Neural Networks and a convolutional discriminator. The network, error metrics and training procedure are adapted to the task of fine-grained sketching. Through quantitative and perceptual experiments, we show that our model outperforms previous work and that our dataset is a valuable benchmark for generative models. We will make our dataset publicly available.

**Keywords:** Generative Adversarial Networks, Recurrent Neural Networks, Sketching, Tree modeling

## 1 Introduction

Generative modelling using deep networks has shown promising results for synthesising visual content [1–8]. The ability to learn visual semantics makes these models very useful for large scale synthesis, *e.g.*, for creating assets for graphics applications or for generating training data for other learning tasks. In this paper, we focus on 2D sketching. While sketching is the most basic content creation task, it is still a challenging problem if fine details need to be produced. The ability to learn how to synthesise fine details from training sketches is thus a key requirement for generative models for sketching.

In order to benchmark generative models for the task of fine-grained sketching, we develop a novel training dataset with complex structures. We choose tree skeletons as the shape class for our benchmark (*c.f.* Fig. 1). This is in contrast to the popular choice of man-made objects like tables, chairs *etc.* in other datasets. Our motivation is two fold. First, tree modelling is very relevant to high quality

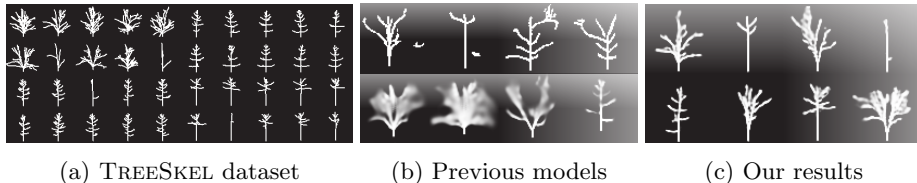


Fig. 1: Synthesising fine-detailed structures via generative models is an interesting problem. We propose new and challenging dataset TREE SKEL in the form of 2D trees (a). We also propose a novel generative model SKETCHGEN, that produces significantly more realistic trees (c) compared to state-of-the-art (b).

graphics applications and remains a difficult problem in spite of a long line of research [9–20]. Being able to learn a generative model for trees thus helps to solve a real-world problem. Secondly, trees are an interesting shape class. They have fine organic details which are hard to capture for methods tested on structured man-made objects. We show that state-of-the-art generative models that produce good results on simple datasets like MNIST hand-drawn digits fail to generate satisfactory results on our dataset (*c.f.* Fig. 1). This highlights the need for challenging benchmarks for freeform sketching such as the benchmark we propose in this paper.

Motivated by the deficiencies of existing generative models, we propose a new approach able to replicate fine details (*c.f.* Fig. 1). We use a Recurrent Neural Network (RNN) to synthesise tree sketches from random points in a low dimensional space, inspired by DRAW [21]. The RNN colours pixels sequentially and connects coloured pixels by varying the size of attention window to preserve details. We use the RNN as the encoder and decoder of a variational autoencoder that learns a meaningful low dimensional manifold from training tree images. This allows generating trees from a particular species as well as interpolating between species. It also allows reconstructing an exemplar tree sketch. We train the network in an unsupervised adversarial fashion using a Convolutional Neural Network (CNN) as discriminator.

In summary, this paper makes the following contributions: We propose a novel dataset to benchmark the ability of a generative model to capture fine details in 2D sketching together with an evaluation protocol based on improved error metrics. We also propose a network architecture for sketching, together with strategies to alleviate training problems. We perform extensive quantitatively and perceptual comparisons of our results with previous models and show that our models is better at recovering fine details. Moreover, our network can learn other classes of shapes, as demonstrated on MNIST digits.

We will make our new dataset, together with the evaluation protocol, publicly available.

## 2 Related Work

Generative modelling refers to neural networks that learn the visual or structural layout of the input and synthesise previously unseen similar samples. GAN [22] is a promising tool for unsupervised learning of images/shapes in generative models. It uses a *discriminator* to judge the quality of samples synthesised by the *generator*. Recent work has improved training [23,24] and evaluation [25].

A variety of network architectures have been tested for generative modelling in various contexts. Dosovitskiy *et al.* [1] used CNNs to generate images of chairs from metadata like view, transformation etc. This was improved with GANs to generate natural images from random low dimensional points [2]. Larsen *et al.* [3] improve this by adding an autoencoder [26] which also learns an explicit low dimensional space. This enables reconstruction [5,27–29] and exploration of shape space [30]. Conditional generation is described using autoencoders [31] and GANs [6,7]. They can learn multiple classes and generate samples of a particular class by accepting a class label along with input samples. Latest research on GAN has focused on improving training for natural image synthesis [8]. While all these methods use convolutional networks, Recurrent Neural Networks (RNN) [32,33] have recently been shown to be useful for causal pixel synthesis, for digits [21], natural images [34] and basic 3D shapes [35].

Most relevant to our work are recent generative models: DCGAN [2], VAE-GAN [3] and DRAW [21]. They have shown impressive results for photorealistic and binary images, and 3D shapes. This techniques are generic and a good representative for a majority of research in generative modelling. They are didactic, in that they present a palette of design choices to compare: CNNs, RNNs, adversarial training, autoencoder *etc.*, for designing a new network for a new problem. Subsequent work has added functionality like conditional generation [6,7,31]; our dataset has only one class of shapes, so we do not require conditional generation. We show the results of DCGAN, VAE-GAN and DRAW on our dataset (*c.f.* Sec. 3.1) and design our network after analysing the their artefacts (*c.f.* Sec. 4). We later compare our results to these using quantitative evaluation and perceptual studies (*c.f.* Sec. 5.2).

## 3 TreeSkel: A Large Dataset for Generative Modelling of Fine Details

As one of the main contributions of this paper, we create TREESKEL, a new dataset consisting of tree skeletons. In the following, we motivate our new dataset, describe its creation, and demonstrate that it is challenging for state-of-the-art generative models. We will make this dataset publicly available upon publication.

We decided to create a dataset of trees as they have interesting intra-class variations and exhibit fine details. In addition, a tree-based dataset also address the need for virtual vegetation in graphics applications. TREESKEL consists of 15000 sketches, with 1000 sketches for each of its 15 different tree species. The sketches were created in an artist assisted process described below. TREESKEL



Fig. 2: TREE SKEL creation. From left to right: 3D Larch tree model created in Blender, binary rendering of tree, and tree skeleton after median axis computation. TREE SKEL contains 15000 tree skeletons of 15 species.

is designed as a response to the lack of benchmark datasets for fine grained sketching. Existing datasets in deep learning are geared towards other tasks. For example, CIFAR is designed for object classification [36], ImageNet for image classification [37], and MNIST for handwriting recognition [38]. ImageNet and CIFAR model the distribution of natural images, and MNIST is a collection of natural variations in handwritten digits. While MNIST is a valid training set for sketching, the structure of handwritten digits is rather simplistic. As such, MNIST is not a suitable benchmark to evaluate the ability of generative models to produce fine details. In contrast, TREE SKEL is deliberately curated to teach a network how to sketch fine details and variations. As such, it is similar in spirit to Gharbi *et al.* [39] who proposed a dataset to alleviate specific image processing artefacts. Our dataset is the first that can be used for sketching because:

- it abstracts away texture, lighting, *etc.* and focuses on the skeletal structures most relevant for sketching,
- it is created under controlled conditions to exhibit fine details and a large gamut of variations so as to test a generative model’s expressive ability,
- it contains equal number of samples of each species so as to make the network equally proficient at all species,
- it resembles real trees so as to retain relevance to applications that require virtual vegetation.

In order to create the dataset, we selected 15 tree species as the classes in TREE SKEL: Acacia, Beech, Callistemon, Cedar, Chestnut, Elm, Japanese Maple, Kauri, Larch, Linden, Pine, Quaking Aspen, Small Maple, Teak and White Birch. These species are sufficiently diverse to test the expressive ability of the network. We asked artists to design one or more 3D tree models for each species using the SAPLING<sup>1</sup> addon in Blender<sup>2</sup>. This is a time consuming process because modelling tools have a number of parameters to tune for a specific appearance. Given the models, we thus added controlled randomisation to each parameter in the modelling tool to automatically generate a large number of tree models. We then render the models from four randomly chosen viewpoints into  $64 \times 64$  binary images (*c.f.* Fig. 2). The viewpoints are placed at average human height with a field of view that captures the entire tree. We extract the medial axis

<sup>1</sup> <https://github.com/abpy/improved-sapling-tree-generator>

<sup>2</sup> <https://www.blender.org/>

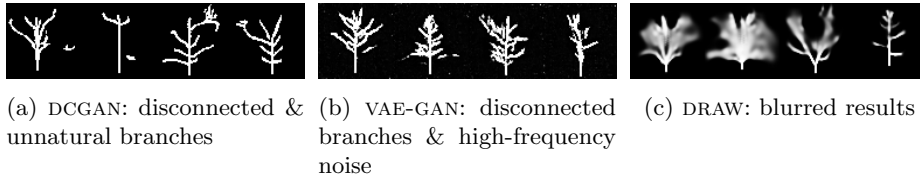


Fig. 3: Evaluation of state-of-the-art generative models on our novel TREESKEL dataset. As can be seen, DCGAN [2], VAE-GAN [3], and DRAW [21] each have distinct failure modes and none of them generates realistic tree sketches.

which represents the tree skeleton. This allows the network to focus on structure; branch thickness can be conveniently handled in post-process if needed. We also restrict the the number of times the trunk splits into branches from the root to the tip of a twig to 2 while creating 3D trees. Higher splitting factors require rendering to image resolutions that are currently computationally intractable for deep networks. These final images constitute the database (*c.f.* Fig. 1). In the following, we refer to samples from TREESKEL as TRAINING and network synthesised samples as GENERATED.

### 3.1 Challenges Contained in The Dataset

In order to demonstrate the challenges inherent to fine-grained sketching of trees that are covered by our dataset, we tested state-of-the-art generative models (*c.f.* Sec. 2) on TREESKEL. Exemplary results from this experiment are shown in Fig. 3: DCGAN [2] produces unnaturally looking structures and disconnected branches (*c.f.* Fig. 3a). VAE-GAN [3] results are better but they have far more disconnected branches, to the point that they resemble high frequency noise (*c.f.* Fig. 3b). These results show that our dataset contains sufficient details that cannot be modelled by a convolutional network that does not synthesise pixels in a causal order. Random structures can pop up and the network has no mechanism to ensure creating a connectivity that resembles valid images. DRAW [21] uses a RNN encoder-decoder to learn a pixel colouring order during sketching. This results in less noise and fewer disconnected branches, but heavily blurs fine details (*c.f.* Fig. 3c). All these artefacts: unnatural structures, disconnected structures, noise, blur *etc.*, are not observed when evaluating on existing datasets such as MNIST digits. TREESKEL is thus a challenging dataset that exposes the limitations of existing generative models.

## 4 SketchGen: A Generative Model

The poor results of previous generative models (*c.f.* Fig. 3) demonstrate the need for a better model. We propose the SKETCHGEN model that is better adapted to fine-grained sketching. Our network consists of three parts. The first is an *encoder* that converts input image into a point in a latent space. The second is a *decoder* that converts a point in latent space back into an image.

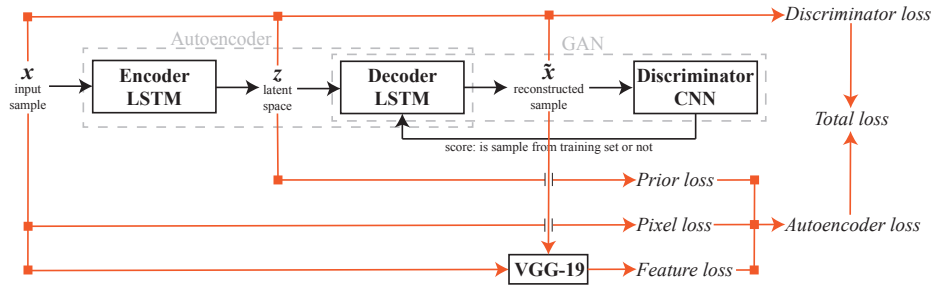


Fig. 4: SKETCHGEN architecture with loss functions.

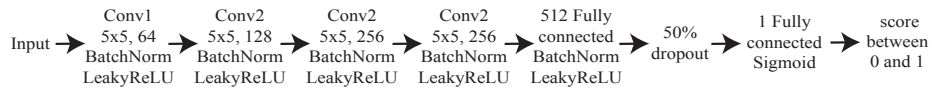


Fig. 5: SKETCHGEN discriminator CNN layers.

The last is a *discriminator* that classifies an image as one belonging to the training dataset or not. The encoder-decoder combine as an *autoencoder* that enables reconstruction, and the decoder-discriminator combine as a GAN that allows unsupervised learning. Our architecture is illustrated in Fig. 4.

An important difference between our network and previous models is that we use a Recurrent Neural Network (RNN) as the encoder and decoder, in contrast to the CNNs used by previous models [1–4, 6–8]. This choice is motivated by the poor sketching results of convolutional decoders on TREESKEL (*c.f.* Fig. 3). We attribute this failure to the lack of pixel colouring order in convolutional networks, which leaves disconnected structures and high frequency noise. An RNN is a promising solution that can learn causal pixel synthesis. Incorporating an autoencoder is consistent with recent generative models because it creates a meaningful latent space that can be used for reconstruction from exemplars. In addition, it enables interpolation in the latent space for controllable synthesis [5, 27–30].

In order to ensure that our synthesised samples contain fine-grained details while still being semantically consistent, *e.g.*, to avoid disconnected branches, we measure both pixel-level difference as well as higher-level feature similarity in our loss functions.

#### 4.1 Network details

Our **encoder** is a LSTM [32] that takes the input sample and the hidden vector output of the previous time step to produce the output of the current time step. The details of the architecture are the same as those in DRAW [21], with different hyperparameters (*c.f.* Table 1). We also incorporate the attention mechanism from DRAW to determine the window of pixels to be sketched at any time step. Our experiments showed better results with the attention mechanism. The **decoder** mirrors the same LSTM architecture.



Fig. 6: Ablation study: results using only feature loss, only pixel loss, and both losses. Only the feature loss can give noisy results and arbitrary pixel values. Using both losses preserves features and gives sharper results than pixel loss alone.

Our **discriminator** is a multi-layer CNN (*c.f.* Fig. 5). All convolutions are  $5 \times 5$  and followed by batch normalisation [40] and leaky ReLU [41]. The convolutional layers are followed by fully connected layers, a 50% dropout layer to prevent overfitting, and a sigmoid that returns the likelihood that the input image belongs to the training dataset. We did not use a very deep network like VGG-19 [42] because our discriminator only has to decide whether binary sketches are from the training dataset or not, which is simpler than VGG’s task of learning natural images.

## 4.2 Loss Functions

We train the autoencoder and the GAN simultaneously. The overall objective is a combination of the autoencoder loss  $\mathcal{L}_E$  and discriminator loss  $\mathcal{L}_D$ :

$$\mathcal{L} = \mathcal{L}_E + \mathcal{L}_D . \quad (1)$$

The autoencoder loss  $\mathcal{L}_E$  ensures that the encoder and decoder are trained such that input images to the encoder and their corresponding decoded outputs retain fidelity. The discriminator loss  $\mathcal{L}_D$  additionally aims to ensure that the output of the decoder is always indistinguishable from training set samples, irrespective of the input to the decoder. Without  $\mathcal{L}_D$ , the only latent space points that can be decoded to images that look like training set are those that are close to encoding of training set images while random points in latent space may decode to arbitrary results.  $\mathcal{L}_D$  is therefore indispensable for synthesising sketches from random latent space points. We now detail the autoencoder loss while the discriminator loss is described at the end of the section.

We formulate the autoencoder loss  $\mathcal{L}_E$  as a combination of three terms, which ensure input-output fidelity and enforce a meaningful latent space:

$$\mathcal{L}_E = \mathcal{L}_{\text{prior}} + \lambda_{\text{pixel}}\mathcal{L}_{\text{pixel}} + \lambda_{\text{feat}}\mathcal{L}_{\text{feat}} . \quad (2)$$

Here,  $\mathcal{L}_{\text{pixel}}$  and  $\mathcal{L}_{\text{feat}}$  are pixel and feature losses which directly measure the fidelity between input image to the encoder and output image of the decoder.  $\mathcal{L}_{\text{prior}}$  is the prior loss which regularises  $\mathcal{L}_{\text{pixel}}$  and  $\mathcal{L}_{\text{feat}}$  such that a meaningful latent space is constructed. Without  $\mathcal{L}_{\text{prior}}$ , the latent space may assume an arbitrary distribution and the purpose of having separate encoder and decoder will be lost.

In the following, we denote the input training samples as  $x$ , and the outputs of the encoder, decoder, and discriminator as  $E[\cdot]$ ,  $G[\cdot]$ , and  $D[\cdot]$ . Using these operators, we can express the latent space conversion of the input image as  $z = E[x]$ , and the reconstruction result as  $\tilde{x} = G[E[x]]$ . We denote a randomly sampled point in latent space as  $z_r$ . We now explain each loss function in detail.

The **prior loss**  $\mathcal{L}_{\text{prior}}$  regularises the encoder by enforcing a probability distribution known *a priori* on the latent space. We enforce a zero mean Gaussian distribution. As formulated by Kingma & Welling [43], we compute the analytic KL-divergence between the  $k$ -dimensional latent space  $p(z|x)$  and the prior  $\mathcal{N}(\mathbf{0}, \mathbf{I})$  using the mean  $\mu$  and covariance matrix  $\Sigma$  of the observed latent space:

$$\mathcal{L}_{\text{prior}} = \frac{1}{2} (\text{tr}(\Sigma) + \mu^T \mu - k - \log(\det(\Sigma))) \quad . \quad (3)$$

The **pixel loss**  $\mathcal{L}_{\text{pixel}}$  is a direct measure of fidelity between input  $x$  and reconstruction  $\tilde{x}$ . To this end, we use pixel-wise mean squared error.

$$\mathcal{L}_{\text{pixel}} = \|x - \tilde{x}\|_2 \quad . \quad (4)$$

The pixel loss  $\mathcal{L}_{\text{pixel}}$  only accounts for low-level similarity. In order to synthesise realistic tree shapes, it is necessary to also account for higher-level similarity. We thus also use a **high-level feature loss** that accounts for consistent branching behaviour and connectivity. Intermediate representations learnt by classifier CNNs have been shown to encode high-level features that can be used to measure similarity between images [44, 45]. Generative models have also used features extracted from intermediate layers of pre-trained CNNs [3, 4], or discriminator [6]. We extract feature maps as the intermediate activations of a pre-trained VGG-19 network [42]. Let  $V_i$  and  $\tilde{V}_i$  denote the activations of the  $i^{\text{th}}$  convolutional plus ReLU layer of VGG applied to input  $x$  and reconstruction  $\tilde{x}$ , respectively. The feature loss  $\mathcal{L}_{\text{feat}}$  is given by:

$$\mathcal{L}_{\text{feat}} = \frac{1}{N} \sum_{i \in L} \sigma\left(\frac{i}{|L|}\right) \|V_i - \tilde{V}_i\|_2 \quad . \quad (5)$$

Here  $\sigma(\cdot)$  is the sigmoid function,  $N = \sum_i \sigma\left(\frac{i}{|L|}\right)$  is a normalisation factor, and  $L$  is the set of VGG layers whose activation is used.

In order to account for various kinds of features, we use multiple early VGG layers  $L = \{\text{ReLU2}_2, \text{ReLU3}_4, \text{ReLU4}_4, \text{ReLU5}_4\}$ . The progressively increasing sigmoidal weights prioritise semi-global features. This loss preserves structure and alleviates blurring compared to the pixel loss (*c.f.* Fig. 6). However, it alone is not sufficient because it can lead to high frequency artefacts [46]. We combine it with the pixel loss using weights  $\lambda_{\text{feat}} = 10$  and  $\lambda_{\text{pixel}} = 0.5$  in Eq. 2.

Our **discriminator loss** is formulated as Wasserstein GAN objective [24], which reportedly is more stable than the cross-entropy GAN objective used by VAE-GAN:

$$\mathcal{L}_D = \mathbb{E}[-D[x] + D[G[z_r]] + D[\tilde{x}]] \quad . \quad (6)$$



Here,  $\mathbb{E}[\cdot]$  denotes the expectation over all training samples  $x$  in a mini-batch, their corresponding reconstructions  $\tilde{x}$ , and an equal number of randomly drawn points  $z_r$ .

We also include the discriminator result for the decoded training samples  $D[\tilde{x}]$  in Eq. 6, in addition to the usual terms involving  $x$  and  $z_r$ . The intuition is as follows: The traditional  $D[x]$  and  $D[G[z_r]]$  terms measures the ability of the discriminator to judge if the image decoded from a random latent point  $G[z_r]$  is similar to a training image  $x$ . By adding  $D[\tilde{x}]$ , we are judging the quality of the discriminator by its ability to distinguish not only random synthesised samples from training images, but also reconstructions of training samples from training samples themselves. Using this addition improved our results.

### 4.3 Training Details

Training GANs is non-trivial because a discriminator that becomes too powerful too early prevents a proper training of the generator. We alleviate this by selectively training the discriminator so that it never gets too strong compared to the generator [3, 4]. We define a **generator loss**  $\mathcal{L}_G = -\mathbb{E}[D[G[z_r]] + D[\tilde{x}]]$  as the opposite of  $\mathcal{L}_D$  (Eq. 6). We omit the  $x$  term because  $\mathcal{L}_G$  only measures the likelihood of the discriminator being fooled by the decoder. In practice,  $\frac{\mathcal{L}_D}{\mathcal{L}_G}$  should be close to 1, indicating that the generator is not much stronger than the discriminator. We thus skip a discriminator update if

$$|\mathcal{L}_D/\mathcal{L}_G| \geq 1.5 \log(1 + j) \quad , \quad (7)$$

where  $j$  is the number of the current epoch. By choosing the threshold as an increasing function of the training epoch, we ensure that the discriminator parameters are updated rarely in the beginning and frequently afterwards when the generator has received some training. Encoder and decoder parameters are always updated.

In practice, we do not update all network parameters w.r.t. the combined loss (Eq. 1) during optimisation. We update the parameters of the encoder  $\theta_E$  by backpropagating the gradient of the autoencoder loss, the decoder  $\theta_G$  by the autoencoder and generator loss, and the discriminator  $\theta_D$  by its own loss:

$$\theta_E \leftarrow^{\pm} \nabla_{\theta_E} (\mathcal{L}_E) \quad , \quad \theta_G \leftarrow^{\pm} \nabla_{\theta_G} (\mathcal{L}_G + \mathcal{L}_E) \quad , \quad \theta_D \leftarrow^{\pm} \nabla_{\theta_D} (\mathcal{L}_D) \quad . \quad (8)$$

This implementation strategy was also used by Larsen *et al.* [3]. We use ADAM [47] for optimisation with momentum  $\beta_1 = 0.5$ . We also clip the gradient norm at 10 in all losses to avoid exploding gradients because of accumulation over long time sequences in LSTMs [48].

## 5 Evaluation

In the following, we evaluate SKETCHGEN and compare its performance against state-of-the-art methods on our TREESKEL dataset. Sec. 5.1 presents a qualitative evaluation of SKETCHGEN. Sec. 5.2 then provides quantitative results using both automated metrics as well as a user study.

Table 1: Hyperparameters of our approach

<b>Training</b>		<b>Encoder-decoder</b>	
epochs	600	learning rate	$5 \times 10^{-4}$
mini-batch size	100	read attention window	$7 \times 7$
<b>Discriminator</b>		write attention window	$12 \times 12$
learning rate	$10^{-4}$	LSTM time steps	64
leaky ReLU slope	0.2	LSTM hidden vector size	256
batch norm decay	0.9	latent space dimensionality	100



Fig. 7: Reconstruction. Even though SKETCHGEN has never seen the top row samples during training, it can faithfully reconstruct them (bottom).

### 5.1 Qualitative Evaluation

In our qualitative evaluation of SKETCHGEN, we are interested both in a comparison with existing methods as well as a deeper understanding of SKETCHGEN’s abilities, especially its ability to synthesise novel tree samples.

First, we demonstrate the ability of SKETCHGEN’s decoder to reconstruct trees not contained in the training sample. This is shown in Fig. 7, where we first use SKETCHGEN’s encoder to map a previously unseen sample to a point in the latent space and then use the decoder to reconstruct the tree starting from this point. As can be seen, SKETCHGEN faithfully reconstructs these examples.

Fig. 8 shows trees synthesised by SKETCHGEN’s decoder from randomly selected points in the latent space. As can be seen, SKETCHGEN is able to generate tree images with detailed branching structures. Visual inspection shows that these results do not have the implausible branch structures of DCGAN, high-frequency noise of VAE-GAN and blurry structures of DRAW (compare Fig. 3 with Fig. 8). These results clearly show that SKETCHGEN generates more realistically looking trees.

The samples synthesised by SKETCHGEN cover all 15 species, showing that the network is not biased towards any particular shape. However, it remains to be shown that its results are not just simple copies of training samples, but that SKETCHGEN actually learns about plausible tree structures. We demonstrate this through two experiments: First, we generated around 1000 synthetic trees, picked random training samples, and for each sample retained its 10 pixel-wise closest matches among the synthesised trees. Fig. 9a compares training samples with these most similar synthesised trees. As can be seen, each synthesised tree differs from the training samples in details.

As a second experiment, we linearly interpolate between points in the latent space. The endpoints are obtained by passing images of two different species through the encoder. As shown in Fig. 10, SKETCHGEN decodes the interpolated points to plausible tree shapes, showing a gradual change from one species to

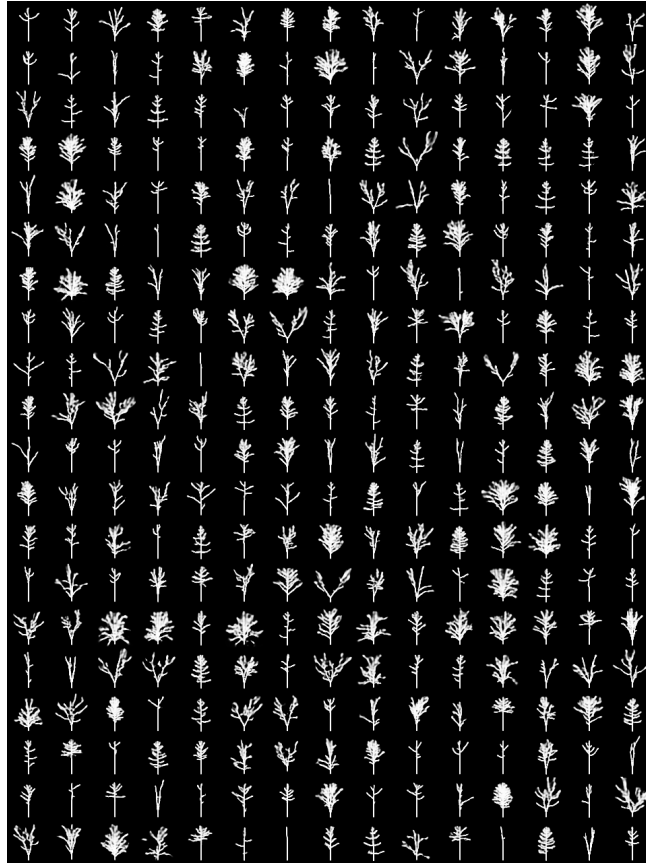
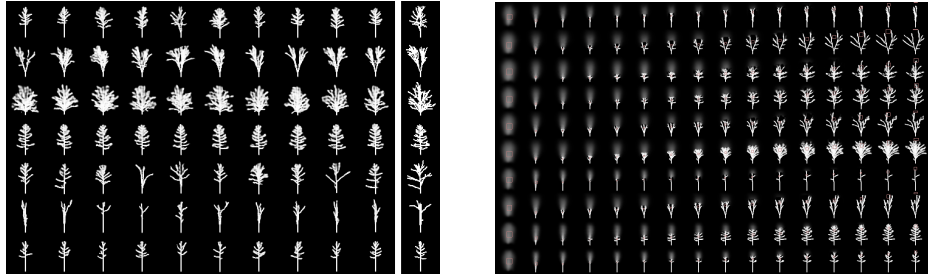


Fig. 8: Samples synthesised by the decoder from random latent space points. Details best viewed at 500% zoom.

another. This clearly demonstrates SKETCHGEN’s ability to automatically learn meaningful relations between the different species.

While the latent space captures high-level structure, fine details are handled by the attention mechanism of the RNN inside the autoencoder. Visualising the sketching sequence over time shows the temporal dependency and evolution of the attention mechanism (*c.f.* Fig. 9b). SKETCHGEN learns this in an unsupervised manner. We also tested SKETCHGEN on MNIST digits [38] and found the results on par with prior models (*c.f.* Fig. 11). This shows that the network architecture of SKETCHGEN generalises to other datasets.

Finally, we perform an ablation study to understand the impact of different parts of our loss function. We obtain the best results using a weighted combination of pixel and feature loss. Using only the feature loss, there is no mechanism to constrain actual pixel values. Thus, a linear or some other transformation of the pixel intensities can give a low feature loss. Using only the pixel loss results in more blur than feature and pixel loss combined. This is because under the



(a) SKETCHGEN does not copy but learns: training samples (right) differ significantly from their 10 most similar randomly generated samples (left).

(b) Temporal sketching by the RNN in SKETCHGEN.

Fig. 9: SKETCHGEN results. Best viewed at 500% zoom.

$\ell_2$  norm, blurry samples still give low pixel losses and there is no mechanism to enforce sharp results. These results are demonstrated in Fig. 6.

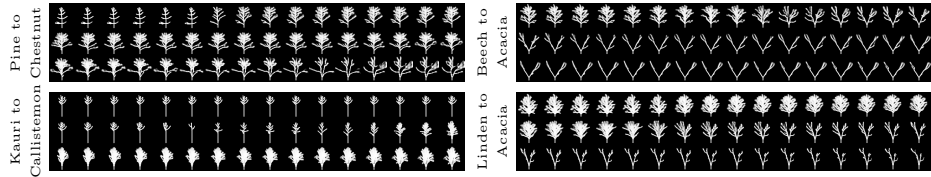


Fig. 10: Latent space interpolation. We choose two random tree samples of different species, map them to the latent space, and show the decoded results from interpolated latent space points. These show that SKETCHGEN learns a meaningful latent space. Best viewed at 500% zoom.

## 5.2 Quantitative Evaluation

In this section, we perform a rigorous evaluation to quantitatively verify the qualitative observation that SKETCHGEN synthesises more realistically looking trees compared to state-of-the-art methods. We show that both machines and humans mistake SKETCHGEN samples more often for training data compared to the other methods.

In the first two experiments, we train a CNN classifier to distinguish between TRAINING samples and those generated by different models. In both cases, we used the LeNet [49] architecture as the CNN of choice; the reason being that we do not want a very deep classifier network so as to avoid overfitting. In the last experiment, we asked human participants to mark samples as TRAINING or GENERATED. For each experiment, we report the false positive rate which is the percentage of GENERATED samples mistaken for TRAINING (*c.f.* Table 2).

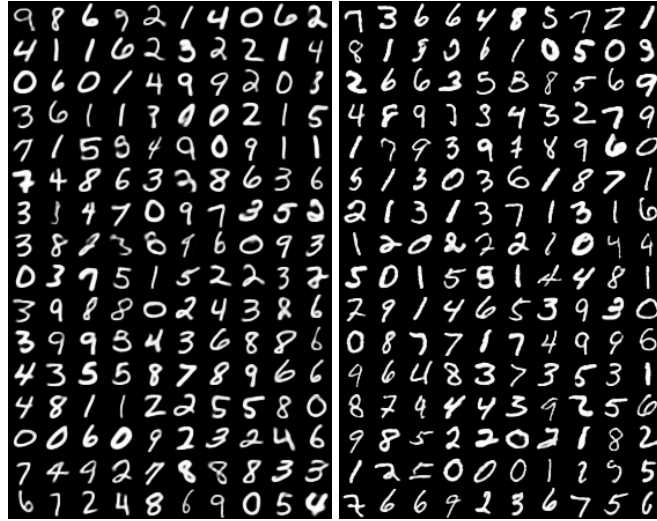


Fig. 11: SKETCHGEN generalises beyond trees. Its results (right) on MNIST digits are on par with the original results in DRAW (left).

Table 2: False positive rates of generative models under different experiments indicating how often GENERATED samples from each method were mistaken for TRAINING. SKETCHGEN results were consistently most indistinguishable from TRAINING samples than other methods.

	DCGAN [2]	VAE-GAN [3]	DRAW [21]	<b>SketchGen</b>
Artefacts study	6.36	9.87	9.65	<b>46.61</b>
Realism study	4.92	3.03	4.38	<b>50.24</b>
User study	33.60	33.17	39.97	<b>52.11</b>

**Quantifying visual artefacts** In the first experiment, we quantitatively show that SKETCHGEN produces less obvious visual artefacts compared to the other approaches. We created a training dataset of 50% TRAINING samples and 50% GENERATED samples selected equally and randomly from the results of DCGAN, VAE-GAN, DRAW and SKETCHGEN. We trained LeNet to classify samples as TRAINING or GENERATED using these labelled images in mini-batches of size 64, learning rate 0.0001, for 200 epochs, such that each epoch corresponds to a full training set pass. The classifier stabilised after training on 3000 labelled samples, learning to recognise the artefacts produced by all models jointly. We tested previously unseen samples of each generative model and report their respective false positive rates. SKETCHGEN results were mistaken for TRAINING almost 50% of the times, compared to less than 20% for previous models (*c.f.* Table 2, first row). This shows that other methods create visual artefacts that are easier to identify for a CNN. In other words, this shows that SKETCHGEN *produces less obvious visual artefacts than previous models*.

**Quantifying realism** The previous experiment demonstrated that SKETCHGEN generates more realistic samples compared to other approaches. However, it does not allow us to measure how realistic these samples are. The second experiment aims to test the realism of the synthesised images by allowing the classifier to focus on the specific artefacts generated by each model. For each model, we trained a separate classifier by training on an equal number of TRAINING and GENERATED images generated by the same model. Thus, the classifier for each model learned to recognise the artefacts produced by the corresponding model. The hyperparameters are the same as for the previous experiment. Table 2 (second row) again shows SKETCHGEN artefacts are *visually less objectionable than those of other methods*.

**Perceptual evaluation** Complimentary to a CNN classifier, we also used human perception to rate the quality of different generative models. We performed an anonymous user study, where we asked participants to judge if a given tree sample is TRAINING or GENERATED. We conducted the study with 26 participants rating a total of 1590 images. The false positive rate shows that SKETCHGEN samples were mistaken for TRAINING samples more frequently than those of the other models (*c.f.* Table 2, third row). Participants also provided subjective feedback that branch connectivity and non-branch-like shapes *e.g.*, blobs were the primary criteria for discerning samples. This study is a useful addition to CNN-based evaluation because humans tend to observe global features while CNNs may be biased by local statistics. Please see the supplemental material for details, screenshots and subjective feedback of the user study.

## 6 Conclusion

In this paper, we have presented TREESKEL, a novel dataset for benchmarking the ability of generative models to synthesise fine details. We have demonstrated that this task is very challenging for existing generative models. We have proposed SKETCHGEN, a network architecture able to better synthesise fine details and avoid visual artefacts, and shown that it produces more realistic results through extensive qualitative and quantitative experiments.

Table 2 suggests that SKETCHGEN almost achieves the theoretically optimal false positive rate of 50%. At the same time, SKETCHGEN still produces some residual artefacts like minor blur, even though significant less than previous methods. While our quantitative experiments thus demonstrate that SKETCHGEN performs better *relative* to existing approaches, they should not be understood as *absolute* measurements. Choosing a network architecture for measuring the absolute false positive rate is still very much an open problem. Still, we believe that our TREESKEL dataset will be helpful when tackling the problem of evaluating the performance of generative models in a self-supervised fashion.

## A Supplementary material

This supplementary material provides additional details on our new TREESKEL dataset, additional qualitative results, and details on our quantitative experiments. These details were left out of the paper due to space constraints.

The remainder of the supplementary material is structured as follows: Sec. A.1 provides additional details on our new dataset. Sec. A.2 shows additional qualitative results. Sec. A.4 analyses the behaviour of our loss functions during training. Sec. A.5 describes details of the setup used for the quantitative experiments presented in Sec. 5.2 in the paper. Finally, Sec. A.6 provides details on the user study we performed to perceptually compare our SKETCHGEN method to existing state-of-the-art generative models.

### A.1 Training data

We will make the proposed TREESKEL dataset publicly available upon publication of the paper. In order to provide a visual overview over the dataset, Fig. 12 shows example trees from the training data. Fig. 13 shows additional examples sorted by tree species.

**Dataset details** The dataset consists of 15000 sample tree skeleton images. There are 15 species with 1000 samples per species. For each species, we asked an artist to create a tree model with Blender using the Sapling addon. These models use a parametric representation. We created 250 different 3D tree models for each species by adding random jitter to the parameters selected by the artist. Rendering each of the 250 models from 4 random viewpoints then resulted in the 1000 samples per species.

### A.2 Additional Qualitative Results

This section provides additional qualitative results for both our proposed SKETCHGEN approach and state-of-the-art generative models.

In addition to Figures 1 and 3 in the paper, Fig. 14 shows trees synthesised using previous generative models. As detailed in the paper, the generated images exhibit different artifacts (disconnected and unnatural branches for DCGAN, disconnected branches and high-frequency noise for VAE-GAN, and blurred images for DRAW).

Figures 8 and 9 in the paper show trees synthesised by our SKETCHGEN method from randomly sampled points in the latent space. Fig. 15 complements these results by randomly perturbing points in the latent space corresponding to training examples. As can be seen, the generated trees seem to appear to correspond to the same species as the training image they were generated from. This suggests that species are clustered in the latent space.

Due to its recurrent nature, our SKETCHGEN method, which is based on an RNN, sketches trees in a temporal way. This is illustrated in the accompanying video.

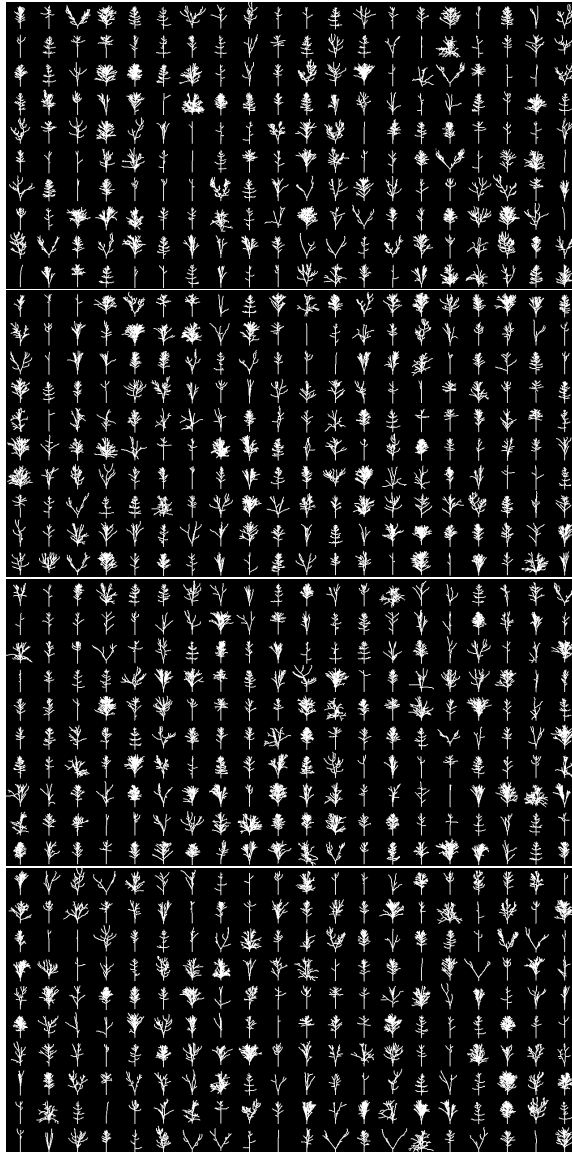


Fig. 12: A visualisation of 800 examples out of the 15000 training samples contained in the proposed TREESKEL dataset.



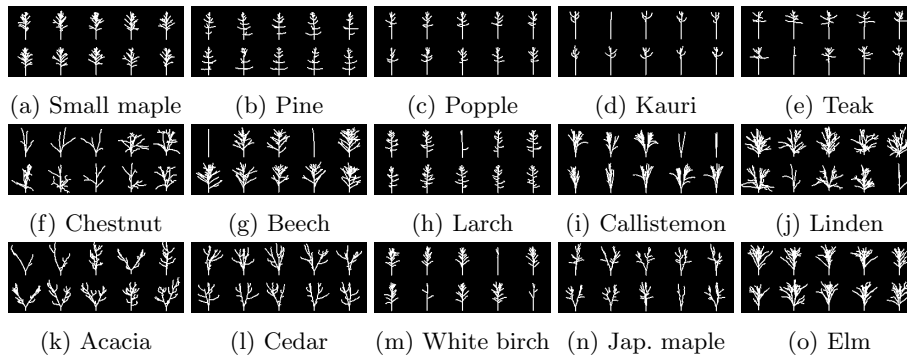


Fig. 13: Examples for the different tree species in contained in the proposed TREESKEL dataset.

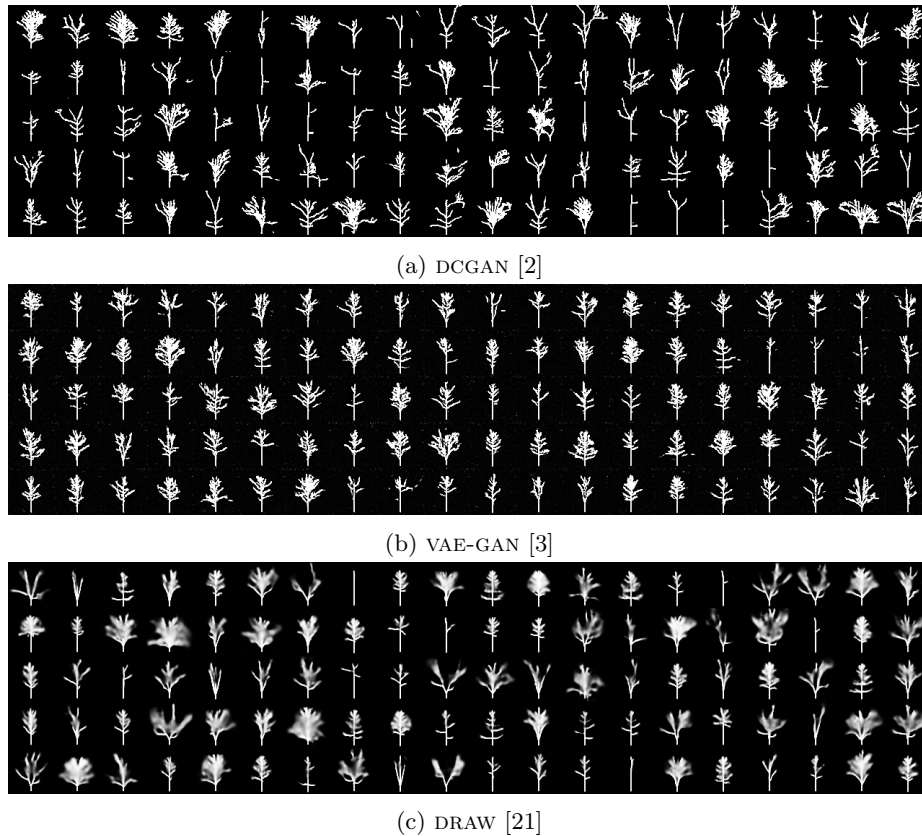


Fig. 14: Results produced by state-of-the-art generative models on our TREESKEL dataset. Notice the different artefacts (disconnected structures, high-frequency noise, and blur) of the different approaches.

### A.3 Prior Methods Implementation Details and Training Parameters

**DCGAN** Our DCGAN implementation is based on the original paper’s [2] proposed network<sup>3</sup>. For our experiments we changed kernel sizes to suite well for the tree skeletons and adapted in-/output channels to grayscale images (see Table 3 for details). For all up- and convolution layers we applied batch normalization, which stabilizes training by shifting the input data to zero mean and unit variance. Note that in the discriminator all *ReLU* activations functions are replaced by *LeakyReLU*. We trained DCGAN on the TREESKEL15K dataset of size  $S_T$  with mini-batches of size  $S_B = 128$ . Using smaller batch sizes leads to unstable training behavior. No pre-processing is performed except for scaling the binarized input images into the range of *tanh* activation function  $[-1, 1]$ . All results are obtained by training with *Adam* optimizer, setting the momentum term  $\beta_1$  to 0.5 and the learning rate to 0.0005. We decreased the learning rate to avoid exploding gradients in the begging of training. For *LeakyReLU* activations we set the slope of the leak to 0.2 as suggested by the authors. The training converges after approximately 180 epochs. An epoch corresponds to  $\frac{S_T}{S_B}$  gradient updates.

Discriminator	Generator
$7 \times 7$ , 64 conv., LeakyReLU	$4 \times 4 \times 256$ , fully-connected, ReLU
$5 \times 5$ , 64 conv., LeakyReLU	$3 \times 3$ , 256 up-conv., ReLU
$3 \times 3$ , 64 conv., LeakyReLU	$3 \times 3$ , 256 up-conv., ReLU
128 fully-connected	$5 \times 5$ , 128 up-conv., ReLU
1 fully-connected, sigmoid	$7 \times 7$ , 64 up-conv. tanh

Table 3: Our DCGAN architecture. We use a different kernel sizes for the discriminator and the generator network.

**VAE-GAN** We implement VAE-GAN based on the proposed framework [3]<sup>4</sup> adapted for binarized images. Table 4 lists details about the encoder and modified discriminator network. The  $l^{th}$ -layer introduced by [3] consists of a weighted sum of different deep convolutional layers. We found that choosing the  $3^{rd}$  and  $4^{th}$  convolutional layers as well as the first fully-connected layer yielded the best results. Similar to [3], we update three optimizers each responsible to minimize either encoder, decoder or discriminator gradients. The hyperparameters remained the same as in the previously presented experiment with DCGAN. If a parameter is not explicitly listed here, it did not change. All learning rates for the encoder, decoder and discriminator are set to 0.0001. The training converges after approximately 450 epochs. An epoch corresponds to  $\frac{S_T}{S_B}$  gradient updates,  $S_T$  denotes dataset size and  $S_B$  is the mini-batch size.

<sup>3</sup> [https://github.com/Newmu/dcgan\\_code](https://github.com/Newmu/dcgan_code)

<sup>4</sup> [https://github.com/andersbll/autoencoding\\_beyond\\_pixels](https://github.com/andersbll/autoencoding_beyond_pixels)

Encoder	Discriminator
5×5, 64 conv., ReLU	5×4, 64 conv., LeakyReLU
3×3, 128 conv., ReLU	3×3, 128 conv., LeakyReLU
3×3, 256 conv., ReLU	3×3, 256 conv., LeakyReLU
256 fully-connected	3×3, 256 conv., LeakyReLU
256 fully-connected	256 fully-connected, LeakyReLU
	50% dropout
	1 fully-connected, sigmoid

Table 4: Our VAE-GAN architecture. Note the generator as listed in Table 3 becomes the decoder network. Encoder as well as discriminator are composed of strided 2D convolutional layers. Dropout is only applied to the discriminator network and acts as a regularization to prevent overfitting.

**DRAW** We follow the approach described in [21]<sup>5</sup>. The model architecture as well as about the used objectives can be found in [21]. We did not change any of the building blocks of DRAW and train the network as proposed with the *Adam* optimizer, the momentum set to  $\beta_1 = 0.9$ . The learning rate is set to 0.0005. Training converges after approximately 300 epoch. An epoch corresponds to  $\frac{S_T}{S_B}$  gradient updates,  $S_T$  denotes dataset size and  $S_B$  is the mini-batch size. All shown samples, we generate from a normal distribution  $z \sim \mathcal{N}(0, 1)$ . We take the same number of dimension for the latent space as suggested in the paper:  $z \in \mathbb{R}^{100}$ . In this experiment we enabled the attention mechanism and set the read and write window size to  $3 \times 3$  and  $5 \times 5$  respectively. The number of glimpses or equivalently defined as time steps, is set to 64. For both recurrent networks, encoder and decoder, we choose the hidden vectors  $h^{enc}$  and  $h^{dec}$  to have dimension 256.

#### A.4 Evaluation of the Loss Functions

Fig. 16 shows the evolution of the different losses as a function of the number of training epochs. Both pixel and feature losses decay slowly as the autoencoder learns to synthesise realistic samples (*c.f.* Fig. 16a). The decreasing discriminator loss indicates that the binary classification of the discriminator improves while the increasing generator/decoder loss illustrates that the generator becomes increasingly more capable of synthesising realistic samples (*c.f.* Fig. 16b).

#### A.5 Evaluation Details

In the following, we expand on the quantitative evaluation presented in Sec. 5.2 of the paper. More precisely, we analyse the impact of using more training samples to train the classifier used for quantitative evaluation.

**Effect of training dataset size on evaluators** A quantitative evaluation using a CNN classifier is valid only if the classifier is well trained. The number

<sup>5</sup> <https://github.com/ericjang/draw>

of labelled images used for training has a direct impact on the quality of the classifier. We visualise classification results of the first CNN based evaluation (titled “Quantifying visual artefacts” in Sec. 5.2 of the paper) as a function of the number of images used to train the classifier (*c.f.* Fig. 17). We observe that the false positive rates stabilise after training the classifier on 3000 or more samples. The quality of the evaluation also increases as the training dataset increases and starts flattening around 3000. For small training sizes, the classifier has the same poor false positive rate, *i.e.*, it is equally confused, for all methods. As the training set size grows, the false positive rate for SKETCHGEN remains close to 50%, while the rates drop steeply for previous methods (*c.f.* Fig. 17). A similar trend was observed for the other CNN based evaluation discussed in Sec. 5.2 in the paper.

**Evaluation on binarised versus grayscale samples** Even though training data for all generative models is binarised, our model and DRAW synthesise grayscale images. During evaluation, a CNN classifier could thus only learn to distinguish between real and synthesised images on the basis on whether they are binary or grayscale. Thus, DCGAN seems to perform best even though it has the worst visual artefacts from a human perspective (*c.f.* Fig. 18a). Our goal is to evaluate high level structure; we therefore binarise all results such that any pixel with intensity 0.6 or higher is snapped to 1, and 0 otherwise. The CNN classifier now learns to distinguish between high level visual content and realism because all images are binary and low level statistics do not dominate the classification (*c.f.* Fig. 18b). As a result, we used the binarised variant for the quantitative results presented in Sec. 5.2 of the paper.

## A.6 User Study Details

This section provides additional details on the user study we used for a perceptual evaluation of the different generative model (*c.f.* Sec. 5.2 in the paper).

**User study setup** We first showed participants 8 examples of TRAINING samples (called *real* in the study) drawn randomly from the TREESKEL dataset, followed by 8 examples of GENERATED samples (called *fake* in the study) drawn randomly from the results of DCGAN, VAE-GAN, DRAW and SKETCHGEN (*c.f.* Fig. 19). Participants were not allowed to return to the 8 *real* and *fake* samples shown at the beginning once they began the classification task. We did not enforce a minimum or maximum on the number of samples each participant had to classify. We upsampled all images to  $128 \times 128$  to aid legibility in the study.

**Subjective feedback** We also asked participants to describe the criteria they used to distinguish between samples. Some of the responses were:

- *not connected white tree parts, not normal shapes of the tree*
- *symmetry, discontinuous branches, orientation of branches, random pixels*
- *disconnected components, thick blobs*
- *fake ones seem to have disconnected far components than the main trunk, and also sometimes unrealistic shapes*

– *too large white blobs. White parts not attached to tree*

These indicate that participants relied on branch connectivity and shapes that do not correspond to realistic branches, *e.g.*, blobs, to distinguish between the samples. This shows that the user study is a useful addition to our CNN-based evaluation because humans tend to observe global features while CNNs may be biased by local image statistics.

## References

1. Dosovitskiy, A., Springenberg, J.T., Brox, T.: Learning to generate chairs with convolutional neural networks. In: IEEE Conference on Computer Vision and Pattern Recognition. (2015) 1538–1546
2. Radford, A., Metz, L., Chintala, S.: Unsupervised representation learning with deep convolutional Generative Adversarial Networks. arXiv:1511.06434 (2015)
3. Larsen, A.B.L., Sønderby, S.K., Larochelle, H., Winther, O.: Autoencoding beyond pixels using a learned similarity metric. In: International Conference on Machine Learning. Volume 48. (2016) 1558–1566
4. Dosovitskiy, A., Brox, T.: Generating images with perceptual similarity metrics based on deep networks. In: Neural Information Processing Systems. (2016) 658–666
5. Wu, J., Zhang, C., Xue, T., Freeman, B., Tenenbaum, J.: Learning a probabilistic latent space of object shapes via 3D generative-adversarial modeling. In: Neural Information Processing Systems. (2016) 82–90
6. Bao, J., Chen, D., Wen, F., Li, H., Hua, G.: CVAE-GAN: Fine-grained image generation through asymmetric training. In: IEEE International Conference on Computer Vision. (2017)
7. Nguyen, A., Clune, J., Bengio, Y., Dosovitskiy, A., Yosinski, J.: Plug & Play Generative Networks: Conditional iterative generation of images in latent space. In: IEEE Conference on Computer Vision and Pattern Recognition. (2017)
8. Odena, A., Olah, C., Shlens, J.: Conditional image synthesis with auxiliary classifier GANs. In: International Conference on Machine Learning. Volume 70. (2017) 2642–2651
9. Lindenmayer, A.: Mathematical models for cellular interactions in development. *J. Theoretical Biology* **18**(3) (1968) 280–315
10. Prusinkiewicz, P., James, M., Měch, R.: Synthetic topiary. In: SIGGRAPH. (1994) 351–358
11. Weber, J., Penn, J.: Creation and rendering of realistic trees. In: SIGGRAPH. (1995) 119–128
12. Shlyakhter, I., Rozenoer, M., Dorsey, J., Teller, S.: Reconstructing 3D tree models from instrumented photographs. *IEEE Computer Graphics and Applications* **21**(3) (2001) 53–61
13. Tan, P., Zeng, G., Wang, J., Kang, S.B., Quan, L.: Image-based tree modeling. *ACM Trans. Graph.* **26**(3) (July 2007)
14. Xu, H., Gossett, N., Chen, B.: Knowledge and heuristic-based modeling of laser-scanned trees. *ACM Trans. Graph.* **26**(4) (October 2007)
15. Neubert, B., Franken, T., Deussen, O.: Approximate image-based tree-modeling using particle flows. *ACM Trans. Graph.* **26**(3) (2007) 88

16. Tan, P., Fang, T., Xiao, J., Zhao, P., Quan, L.: Single image tree modeling. *ACM Trans. Graph.* **27**(5) (2008) 108
17. Livny, Y., Yan, F., Olson, M., Chen, B., Zhang, H., El-Sana, J.: Automatic reconstruction of tree skeletal structures from point clouds. *ACM Trans. Graph.* **29**(6) (2010) 151
18. Longay, S., Runions, A., Boudon, F., Prusinkiewicz, P.: Treesketch: interactive procedural modeling of trees on a tablet. In: *International Symposium on Sketch-based Interfaces and Modeling*. (2012) 107–120
19. Bradley, D., Nowrouzezahrai, D., Beardsley, P.: Image-based reconstruction and synthesis of dense foliage. *ACM Trans. Graph.* **32**(4) (July 2013) 74:1–74:10
20. Chaurasia, G., Beardsley, P.: Editable parametric dense foliage from 3d capture. In: *IEEE International Conference on Computer Vision*. (2017)
21. Gregor, K., Danihelka, I., Graves, A., Rezende, D., Wierstra, D.: DRAW: A recurrent neural network for image generation. In: *International Conference on Machine Learning*. (2015) 1462–1471
22. Goodfellow, I., Pouget-Abadie, J., Mirza, M., Xu, B., Warde-Farley, D., Ozair, S., Courville, A., Bengio, Y.: Generative Adversarial Nets. In: *Neural Information Processing Systems*. (2014) 2672–2680
23. Salimans, T., Goodfellow, I., Zaremba, W., Cheung, V., Radford, A., Chen, X.: Improved techniques for training GANs. In: *Neural Information Processing Systems*. (2016) 2226–2234
24. Arjovsky, M., Chintala, S., Bottou, L.: Wasserstein GAN. *arXiv:1701.07875* (2017)
25. Theis, L., Oord, A.v.d., Bethge, M.: A note on the evaluation of generative models. In: *International Conference on Learning Representations*. (2015)
26. Doersch, C.: Tutorial on variational autoencoders. *arXiv:1606.05908* (2016)
27. Jimenez Rezende, D., Eslami, S.M.A., Mohamed, S., Battaglia, P., Jaderberg, M., Heess, N.: Unsupervised learning of 3D structure from images. In: *Neural Information Processing Systems*. (2016) 4996–5004
28. Girdhar, R., Fouhey, D.F., Rodriguez, M., Gupta, A.: Learning a predictable and generative vector representation for objects. In: *European Conference on Computer Vision*. (2016) 484–499
29. Li, J., Xu, K., Chaudhuri, S., Yumer, E., Zhang, H., Guibas, L.: GRASS: Generative recursive autoencoders for shape structures. *ACM Trans. Graph.* **36**(4) (July 2017) 52:1–52:14
30. Yumer, M.E., Asente, P., Mech, R., Kara, L.B.: Procedural modeling using autoencoder networks. In: *ACM Symposium on User Interface Software & Technology*. (2015) 109–118
31. Sohn, K., Lee, H., Yan, X.: Learning structured output representation using deep conditional generative models. In: *Neural Information Processing Systems*. (2015) 3483–3491
32. Hochreiter, S., Schmidhuber, J.: Long Short-Term Memory. *Neural Comput.* **9**(8) (November 1997) 1735–1780
33. Gers, F.A., Schmidhuber, J.: Recurrent nets that time and count. In: *IEEE-INNS-ENNS International Joint Conference on Neural Networks*. Volume 3. (2000) 189–194
34. Oord, A.v.d., Kalchbrenner, N., Kavukcuoglu, K.: Pixel recurrent neural networks. In: *International Conference on Machine Learning*. (2016)
35. Zou, C., Yumer, E., Yang, J., Ceylan, D., Hoiem, D.: 3D-PRNN: Generating shape primitives with Recurrent Neural Networks. In: *IEEE International Conference on Computer Vision*. (2017)

36. Krizhevsky, A., Hinton, G.: Learning multiple layers of features from tiny images. Technical report, University of Toronto (2009)
37. Russakovsky, O., Deng, J., Su, H., Krause, J., Satheesh, S., Ma, S., Huang, Z., Karpathy, A., Khosla, A., Bernstein, M., Berg, A.C., Fei-Fei, L.: ImageNet Large Scale Visual Recognition Challenge. *J. Comput. Vision* **115**(3) (2015) 211–252
38. LeCun, Y., Cortes, C.: The MNIST database of handwritten digits. <http://yann.lecun.com/exdb/mnist/> (2015) Last accessed 2017-05-14.
39. Gharbi, M., Chaurasia, G., Paris, S., Durand, F.: Deep joint demosaicking and denoising. *ACM Trans. Graph.* **35**(6) (November 2016) 191:1–191:12
40. Ioffe, S., Szegedy, C.: Batch normalization: Accelerating deep network training by reducing internal covariate shift. In: International Conference on Machine Learning. Volume 37. (2015) 448–456
41. Maas, A.L., Hannun, A.Y., Ng, A.Y.: Rectifier nonlinearities improve neural network acoustic models. In: International Conference on Machine Learning. (2013)
42. Simonyan, K., Zisserman, A.: Very deep convolutional networks for large-scale image recognition. In: International Conference on Learning Representations. (2015)
43. Kingma, D.P., Welling, M.: Autoencoding variational bayes. In: International Conference on Learning Representations. (2014)
44. Aittala, M., Aila, T., Lehtinen, J.: Reflectance modeling by neural texture synthesis. *ACM Trans. Graph.* **35**(4) (July 2016) 65:1–65:13
45. Gatys, L.A., Ecker, A.S., Bethge, M.: Image style transfer using convolutional neural networks. In: IEEE Conference on Computer Vision and Pattern Recognition. (2016) 2414–2423
46. Mahendran, A., Vedaldi, A.: Visualizing deep convolutional neural networks using natural pre-images. *J. Comput. Vision* **120**(3) (2016) 233–255
47. Kingma, D.P., Ba, J.L.: ADAM: A method for stochastic optimization. In: International Conference on Learning Representations. (2015)
48. Pascanu, R., Mikolov, T., Bengio, Y.: On the difficulty of training recurrent neural networks. In: International Conference on Machine Learning. (2013)
49. Bottou, L., Cortes, C., Denker, J.S., Drucker, H., Guyon, I., Jackel, L.D., LeCun, Y., Muller, U.A., Sackinger, E., Simard, P., et al.: Comparison of classifier methods: A case study in handwritten digit recognition. In: Pattern Recognition, 1994. Vol. 2-Conference B: Computer Vision & Image Processing., Proceedings of the 12th IAPR International. Conference on. Volume 2., IEEE (1994) 77–82

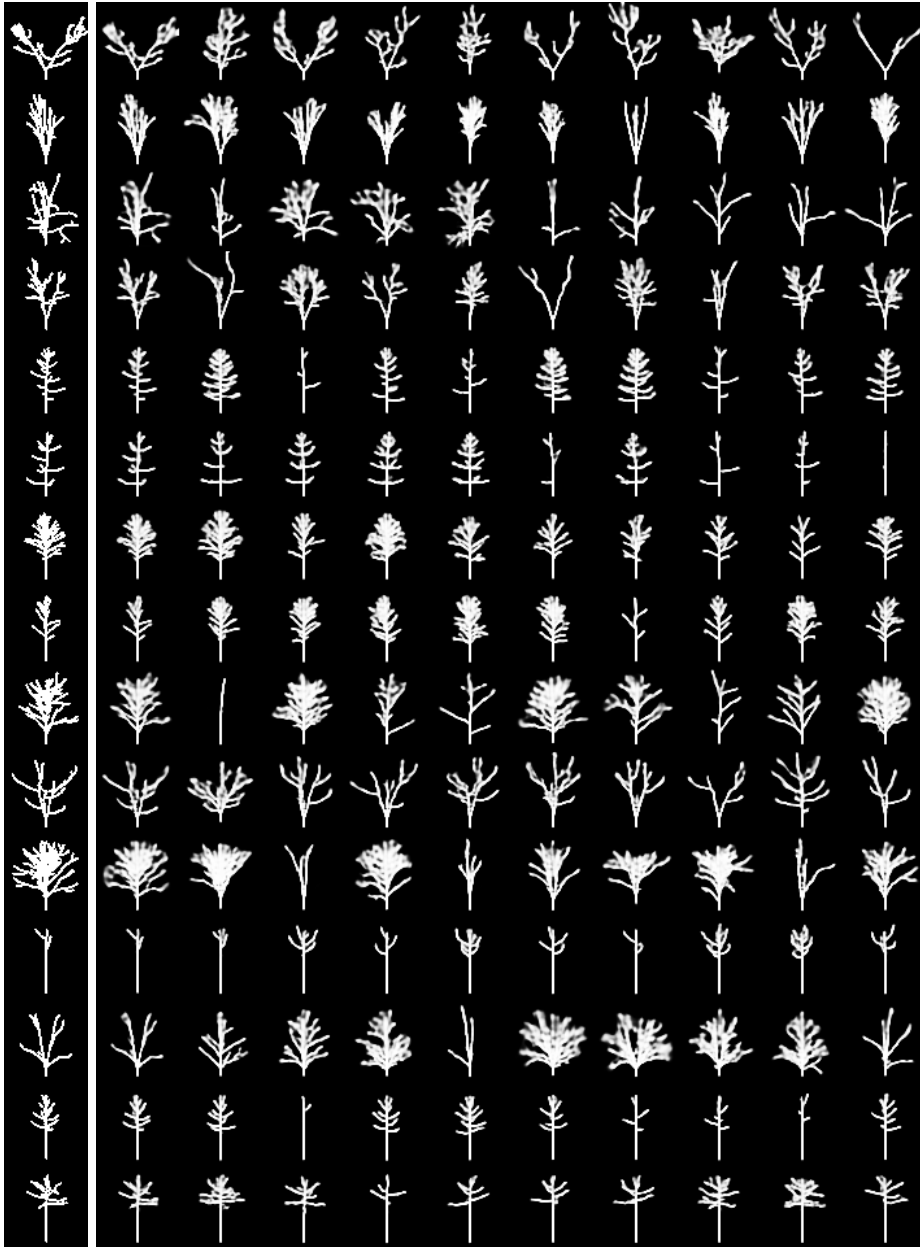
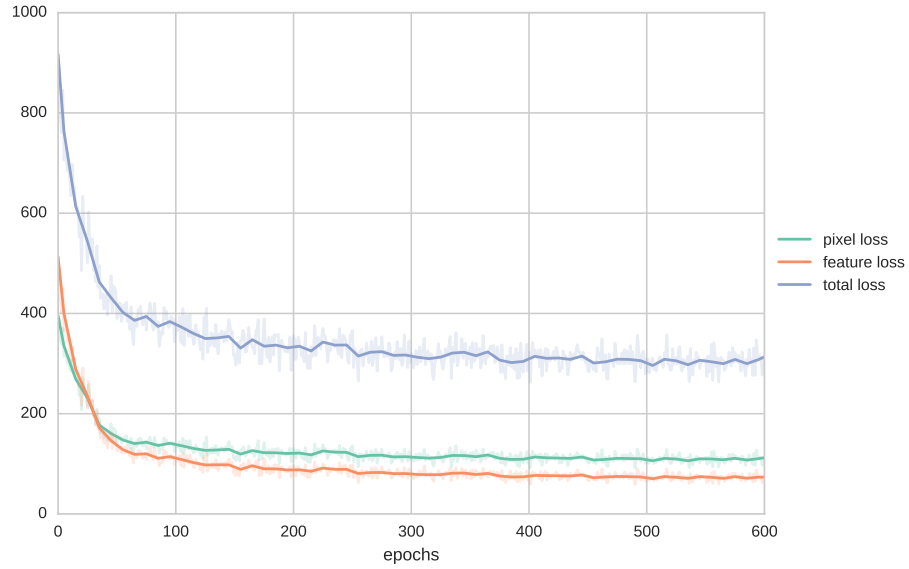
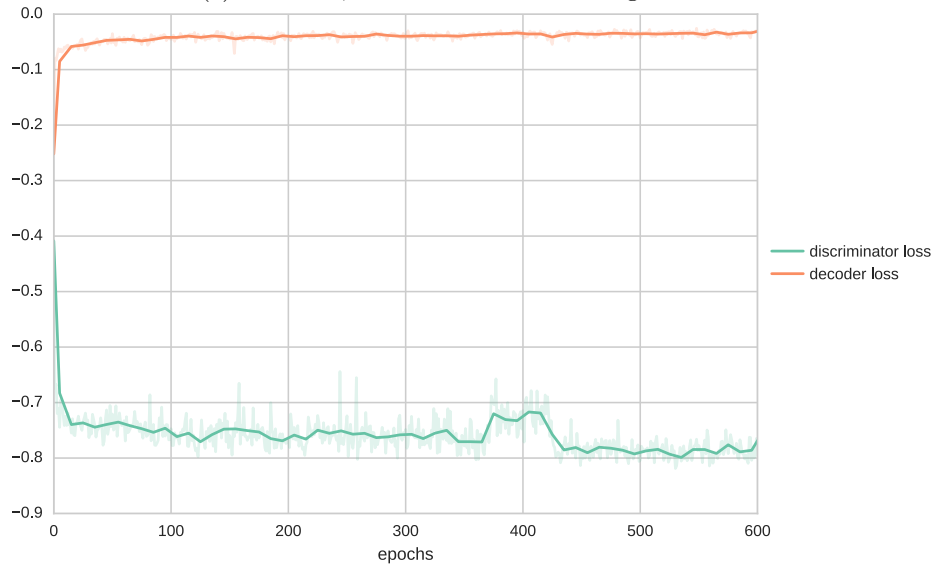


Fig. 15: Species specific synthesis produced by the proposed SKETCHGEN method. Training sample of a species (left) and samples synthesised (right) by adding small perturbation to the latent space encoding of the training sample. The results appear to be same species, which suggests that species may be clustered in latent space.





(a) Pixel loss, feature loss and their weighted sum

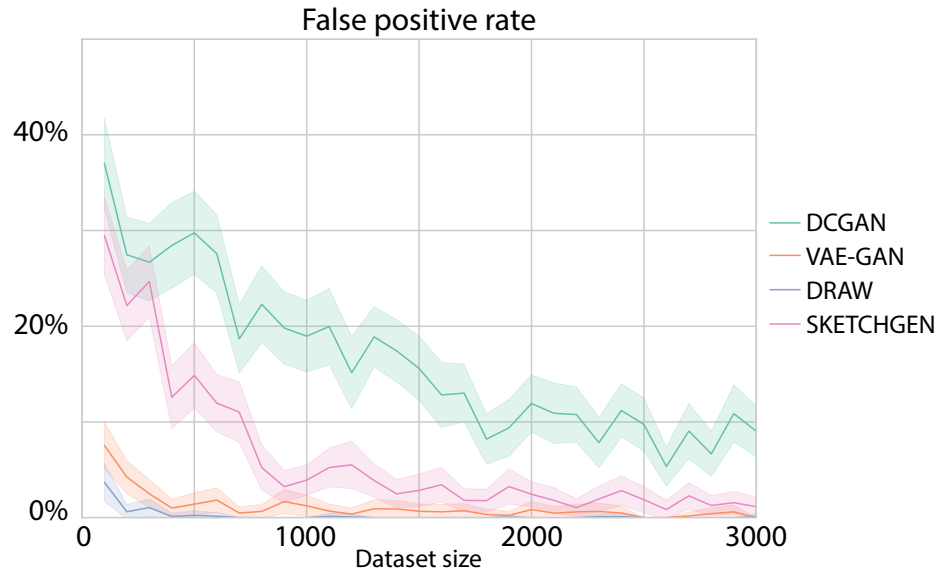


(b) Discriminator and generator or decoder losses

Fig. 16: Evolution of the different loss functions as a function of the number of training epochs.



Fig. 17: Effect of training dataset size on CNN classifier quality for the quantitative evaluation of SKETCHGEN results.

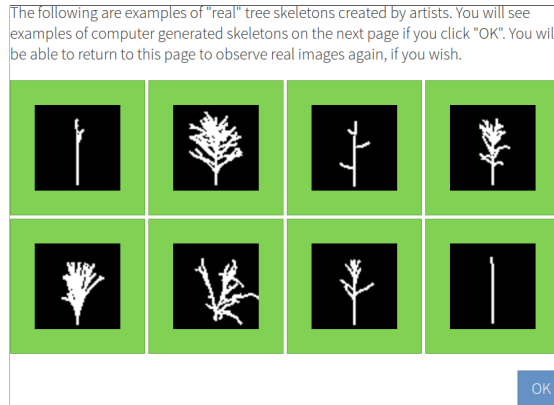


(a) Evaluation on grayscale results

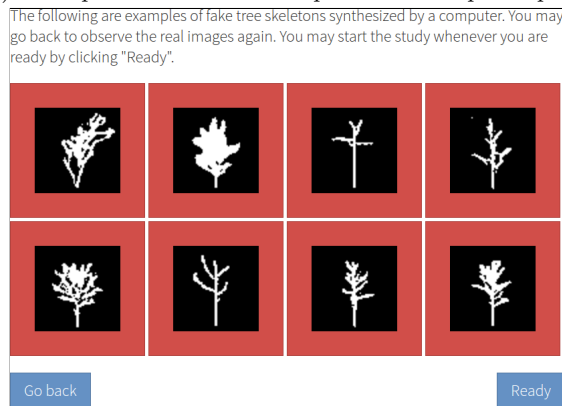


(b) Evaluation on binarised results

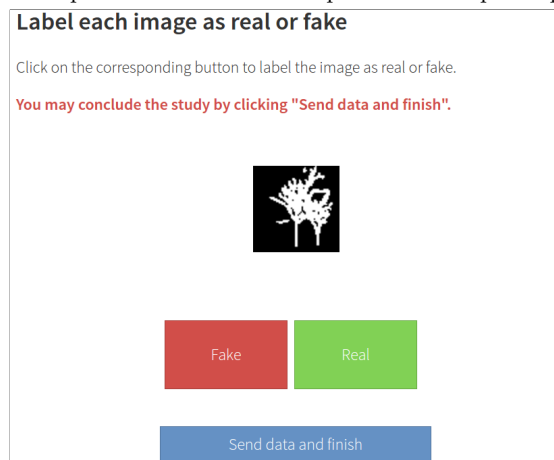
Fig. 18: Evaluation on binarised versus grayscale results.



(a) Examples of TRAINING samples shown to participants



(b) Examples of GENERATED samples shown to participants



(c) Classification task

Fig. 19: Screenshots from our user study.